We are IntechOpen, the world's leading publisher of Open Access books Built by scientists, for scientists

4,800
Open access books available

122,000
International authors and editors

135M
Downloads

Our authors are among the

154
Countries delivered to

TOP 1%
most cited scientists

12.2%
Contributors from top 500 universities

CLARIVATE ANALYTICS BOOK CITATION INDEX INDEXED

WEB OF SCIENCE™

Selection of our books indexed in the Book Citation Index in Web of Science™ Core Collection (BKCI)

Interested in publishing with us?
Contact book.department@intechopen.com

Numbers displayed above are based on latest data collected.
For more information visit www.intechopen.com

1

Ultra-Wideband Waveform Generation Using Nonlinear Propagation in Optical Fibers

Avi Zadok[1], Daniel Grodensky[1], Daniel Kravitz[1], Yair Peled[2], Moshe Tur[2], Xiaoxia Wu[3] and Alan E. Willner[3]
[1]*Bar-Ilan University*
[2]*Tel-Aviv University*
[3]*University of Southern California*
[1,2]*Israel*
[3]*USA*

1. Introduction

Ultra-wideband (UWB) radio is a transmission technology that is based on short pulses, whose spectral width is on the order of several GHz. UWB signals are free of sine-wave carriers, and their duty cycle and power spectral density are low. These characteristics provide UWB radio with unique advantages: improved immunity to multi-path fading, increased ranging resolution, large tolerance to interfering legacy systems, enhanced ability for penetrating obstacles, and low electronic processing complexity at the receiver. UWB technology is considered attractive for a myriad of applications, including high-speed internet access, sensor networks, high accuracy localization, precision navigation, covert communication links, ground-penetrating radar, and through-the-wall imaging (Yang & Giannakis, 2004).

Of the various potential UWB radio applications, much attention has turned to wireless personal area networks, which address short-range, ad-hoc, and high-rate connectivity among portable electronic devices. UWB radio is among the standards that are being considered to replace cables in such networks, due to its multi-path and interference tolerance, low power, and high efficiency. Research efforts in this area have intensified since 2002 when the United States Federal Communication Commission (FCC) allocated the frequency range of 3.6-10.1 GHz for unlicensed, UWB indoor wireless communication (Federal Communications Commission [FCC], 2002). Interest is not limited to indoor wireless communication only: the FCC report relates to imaging systems and vehicular radar systems as well (FCC, 2002). The vehicular radar standard, in particular, specifies a high central frequency of 24 GHz or higher (FCC, 2002). The electronic generation of complex UWB waveforms at such high frequencies is increasingly challenging.

The FCC standard imposes several limitations on the transmitted signals. First, the power spectral density must comply with complicated spectral masks (FCC, 2002). In addition, the total signal power is severely restricted, limiting the range of UWB indoor wireless transmission, for example, to only 10-15 m. In many scenarios, UWB radio-based systems would need to extend their wireless transmission range by other distribution means. As the

frequencies of UWB signals continue to increase, with 100 GHz transmission already reported (Chow et al., 2010), optical fibers become the preferable distribution medium. With radio-over-fiber integration on the horizon, the generation of the UWB pulses by photonic methods becomes attractive. Microwave-photonic generation techniques can offer flexible tuning of high-frequency pulse shapes, inherent immunity to electromagnetic interference, and parallel processing via wavelength division multiplexing (Capmany et al., 2005). Driven by the promises of integration and flexibility, much research effort has been dedicated to photonic generation of UWB waveforms in recent years.

Most microwave-photonic UWB generation schemes thus far target *impulse radio* implementations: the transmission of tailored short pulses and their subsequent coherent detection. One category of photonic UWB generation techniques relied on the conversion of phase to intensity modulation (Yao et al., 2007; Zeng & Yao, 2006; Zeng et al., 2007). This method is simple to implement, however it offers few degrees of freedom for pulse shaping and minimal reconfiguration. Waveforms generated using this method are restricted to a Gaussian mono-cycle or a Gaussian doublet shape. Higher-order pulse shapes were generated based on microwave-photonic tapped delay line filters, with both positive and negative coefficients (Bolea et al., 2009; Bolea et al., 2010). Pulse generation based on four-coefficient filters had been demonstrated (Bolea et al., 2009), however each additional coefficient required an extra laser source.

Another interesting approach is based on nonlinear dynamics in semiconductor optical amplifiers (SOAs) and laser diodes. Cross-gain modulation (XGM) effects in SOAs and cross-absorption effects in electro-absorption modulators had been used in Gaussian monocycle and doublet waveform generation (Ben-Ezra et al., 2009; Wu, et al., 2010; Xu et al., 2007a, 2007b). Relaxation oscillations in directly-modulated or externally-injected distributed feedback lasers were recently demonstrated as well (Gibbon et al., 2010; Pham et al., 2011; Yu et al., 2009). The technique is well suited to the FCC spectral mask for indoor wireless communication: wireless transmission of 3.125 Gbits/s, employing high-order waveforms, had been experimentally demonstrated (Gibbon et al., 2010; Pham et al., 2011). On the other hand, waveform generation based on relaxation oscillations is restricted to the order of 10 GHz by the laser diode dynamics.

The most elaborate waveform tailoring was provided by optical spectrum shaping and subsequent frequency-to-time mapping (Abtahi et al., 2008a, 2008b, 2008c; McKinney et al., 2006; McKinney, 2010). These techniques relied on careful spectral shaping of the transmitted waveforms in order to maximize the transmitted power within the constraints of the FCC mask. However, the demonstrations required mode-locked laser sources, and either bulky free-space optics (McKinney et al., 2006; McKinney, 2010) or highly complex fiber gratings with limited tuning (Abtahi et al., 2008a, 2008b, 2008c). Major progress had been recently achieved, with the pulse-shaping optics successfully replaced by a programmable, integrated silicon-photonic waveguide circuit (Khan et al., 2010).

Nonlinear propagation effects in optical fibers are powerful tools for optical signal processing. However, they have been seldom used in UWB pulse generation research. Li and coauthors used cross-gain modulation in an optical parametric amplifier to generate monocycle and doublet pulse shapes (Li et al., 2009). Velanas and coauthors used a cross-phase-modulation (XPM) based technique to obtain monocycle shapes (Valenas et al., 2008). Both schemes required two input laser sources.

In the first section of this work, we use nonlinear propagation of a pulse train from a single laser source for the generation of high-order UWB impulse radio waveforms (Zadok et al.,

2009; Zadok et al., 2010a, 2010b, ©2010 IEEE). All-optical edge detectors of the input pulses intensity are used to generate two temporally-narrowed replicas of the input pulse train. The edge detection relies on the time-varying chirp introduced by self-phase modulation (SPM), and judiciously tuned optical filters. SPM accumulates through propagation along sections of fiber, which can also serve for the distribution of pulses from a network terminal to a remote antenna element. The shapes of the narrowed replicas are subtracted from that of the original pulse train in a broadband, balanced differential detector. The resulting waveforms are highly reconfigurable through adjustments of the input power and tuning of the optical filters. High-order UWB waveforms, having a center frequency of 34 GHz and a fractional bandwidth of 70% are generated.

UWB architectures that are based on impulse radio require elaborate pulse shaping and a detailed knowledge of the communication channel properties (Qiu et al., 2005; Yang & Giannakis 2004). A possible alternative is the transmission of modulated, broadband noise waveforms. One such implementation relies on direct energy detection (Sahin et al., 2005). Incoherent detection, however, compromises the immunity to interference of UWB technology. Coherent detection can be restored using transmit-reference (TR) schemes, in which the modulated noise is accompanied by a delayed, unmodulated replica of itself (Narayanan & Chuang, 2007). Data is recovered by a matched delay at the receiver end (Narayanan & Chuang, 2007), and knowledge of the channel response is not required (Sahin et al., 2005). Photonic generation of UWB noise has been demonstrated recently, based on the chaotic dynamics of a laser diode in a feedback loop (Zheng et al., 2010).

In the second part of this work we propose, analyze and demonstrate the photonic generation of UWB noise, based on the amplified spontaneous emission associated with stimulated Brillouin scattering in optical fibers (SBS-ASE) (Peled et al., 2010, ©2010 IEEE). The noise bandwidth is extended to 1.1 GHz, using a recently proposed method for broadening of the SBS process (Zadok et al., 2007). Gaussian noise of such bandwidth can be readily generated electrically, however photonic generation techniques are appealing from a radio-over-fiber integration standpoint (Yao et al., 2007). Both direct detection and TR-assisted coherent detection are demonstrated. The performance is in agreement with the theoretical analysis.

Finally, as noted above, UWB waveforms find applications in various radar systems. Noise-based waveforms, in particular, provide better immunity to interception and jamming (Chuang et al., 2008; Narayanan, 2008). Similarly to UWB communication, photonic techniques could provide flexible and reconfigurable generation of broadband, high-carrier frequency noise waveforms, integrated with simple long-reach distribution. In the last section of this work, we show preliminary ranging measurements of metal objects based on SBS-ASE noise waveforms.

2. UWB impulse radio generation using self-phase modulation in optical fibers

2.1 Self-phase modulation based edge detection

Consider the optical field $E_{in}(t)$ of an input train of super-Gaussian pulses (Zadok et al., 2010b, ©2010 IEEE):

$$E_{in}(t) = \sum_n \sqrt{P_{in}} \exp\left[-\left[\left| t - nT_0 \right| \Big/ 2\tau_0 \right]^m \right] \exp\left(j\omega_0 t \right), \tag{1}$$

with a peak power level P_{in}, central optical frequency ω_0, width parameter τ_0 and pulse separation T_0. The parameter *m* determines the exact shape of the input pulses, and *t* denotes time. In propagating along a highly nonlinear fiber (HNLF) of length *L* [km] and negligible dispersion, the optical field undergoes SPM:

$$E_{HNLF}(t) = E_{in}(t)\exp\left[j\varphi(t)\right] = E_{in}(t)\exp\left[j\gamma L\left|E_{in}(t)\right|^2\right] \tag{2}$$

where γ [W · km] $^{-1}$ is the nonlinear coefficient of the fiber. The nonlinearly induced phase modulation $\varphi(t)$ represents an effective temporally-varying shift of the optical frequency (chirp):

$$\Delta f_{pulse}(t) = \frac{1}{2\pi}\frac{d\varphi(t)}{dt} = \frac{\gamma L}{2\pi}\frac{d\left|E_{in}(t)\right|^2}{dt} \tag{3}$$

Figure 1 shows the instantaneous power $\left|E_{in}(t)\right|^2$ of a single input super-Gaussian pulse with *m* = 5 (top panel), and the corresponding $\Delta f_{pulse}(t)$ for a 1 km-long HNLF with γ = 11.3 [W · km] $^{-1}$ (bottom panel). The leading (trailing) edge of the pulse is associated with a positive (negative) frequency shift. Edge detection of $E_{HNLF}(t)$ is implemented by an optical bandpass filter (BPF) of spectral width 2δ, detuned from ω_0 by a frequency offset $\Delta\omega > \delta > 0$. The BPF would block most of the waveform, except for a segment of sufficient SPM: $2\pi \cdot \Delta f_{pulse}(t) > \Delta\omega - \delta$. As seen in equation (3), this segment corresponds to the leading edge of the pulse. The BPF therefore represents an all-optical intensity edge detector. The details of the narrowed replica of the pulse at the BPF output are determined by its spectral width and detuning as well as the input power P_{in}. The endpoints of the filtered waveform $t_{1,2}$ are approximately given by: $d\left|E_{in}(t_{1,2})\right|^2 / dt = (\Delta\omega - \delta)/\gamma L$. The trailing edge can be filtered in a similar manner, with $\Delta\omega < 0$, $|\Delta\omega| > \delta > 0$. Figure 2 shows the instantaneous power $\left|E_{\pm}(t)\right|^2$ at the output of two 75 GHz-wide BPFs, whose central frequencies are detuned from ω_0 by $\Delta\omega_{\pm}/2\pi$ = ± 135 GHz, respectively. As expected, the filtered waveforms emphasize the pulse edges, and both are narrower than the original input pulse. The shape of the two narrowed replicas can be subtracted from that of the original pulse to generate an UWB waveform, as described next.

2.2 UWB waveform generation using all-optical edge detectors

Figure 3 shows a schematic drawing of a setup for UWB waveform generation, based on all-optical edge detection (Zadok et al., 2010b, ©2010 IEEE). The input super-Gaussian pulse train is split in two branches. The upper branch includes a high-power erbium-doped fiber amplifier (EDFA) and an HNLF section. At the HNLF output, the spectrally broadened pulses are split into two paths once again, and the light in each path is filtered by an individually tunable BPF: one is tuned to detect the pulse leading edge as discussed above, whereas the other is adjusted as a trailing edge detector. The power level of each of the two pulse train replicas is individually adjusted by a variable optical attenuator (VOA). In addition, the relative delay between the two pulse trains can be modified by a tunable delay line (TDL). The two pulse trains are then joined together and directed to the negative port of a balanced, differential detector. Since the difference between the central frequencies of the two replicas is outside the detector bandwidth, beating between the two is largely avoided.

A reference pulse train, arriving from the lower branch of the setup, is detected at the positive port of the balanced detector. The relative delay and magnitude of the reference pulse train are controlled by a second EDFA and TDL.

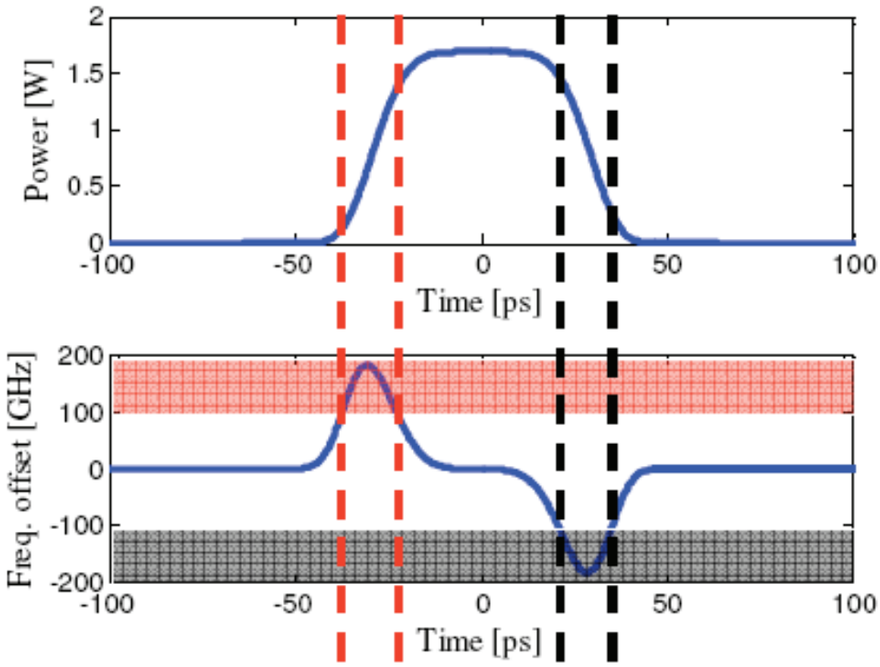

Fig. 1. Top - instantaneous power of an input super-Gaussian pulse: m = 5, τ_0 = 27 ps, P_{in} = 1.7 W. Bottom – simulated SPM-induced instantaneous frequency shift $\Delta f_{pulse}(t)$: L = 1 km, γ = 11.3 [W·km]$^{-1}$. Horizontal shaded regions in the bottom panel schematically denote the passbands of two detuned optical filters. Vertical dashed lines schematically illustrate the temporal edges of the corresponding waveforms at the filters output. ©2010 IEEE.

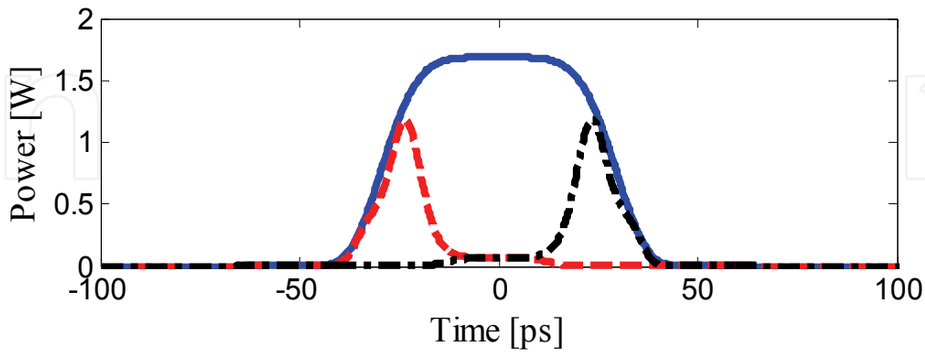

Fig. 2. Solid - instantaneous power of an input super-Gaussian pulse (same as top panel of Fig. 1). Dashed – simulated instantaneous pulse power following propagation in a HNLF and filtering by a 75 GHz-wide BPF, detuned from ω_0 by $\Delta\omega_+/2\pi$ = 135 GHz. HNLF parameters are the as those in the bottom panel of Fig. 1. Dashed-dotted – same as dashed curve, with the BPF detuned from ω_0 by $\Delta\omega_-/2\pi$ = -135 GHz. ©2010 IEEE.

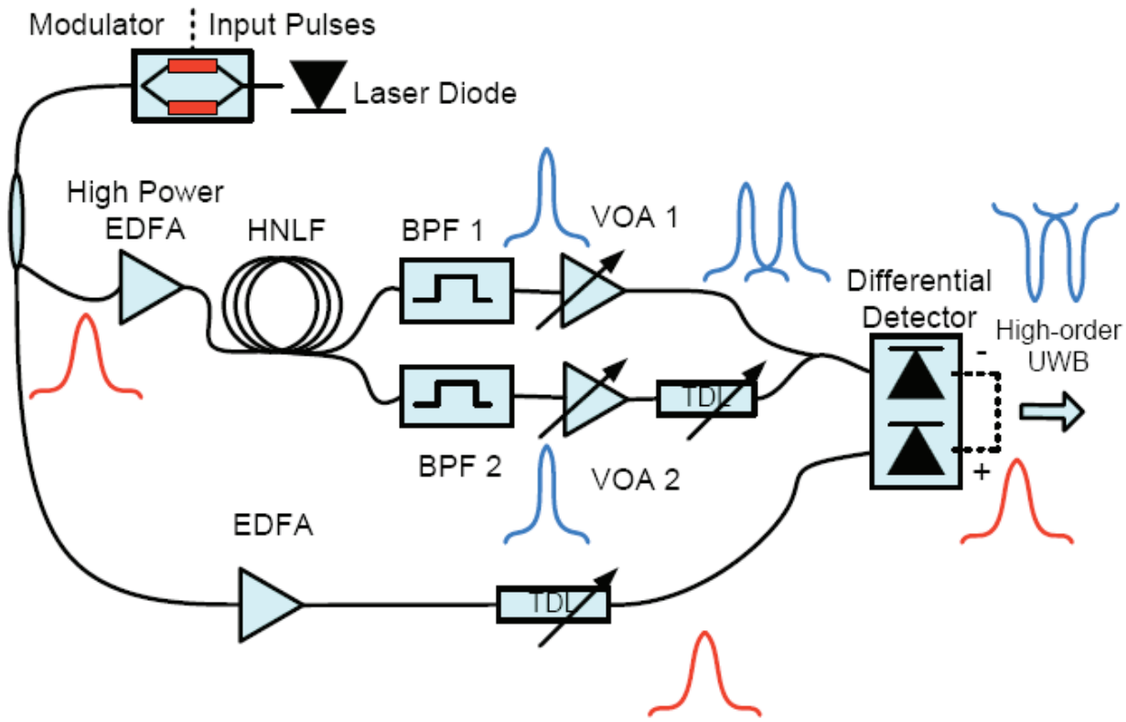

Fig. 3. A schematic diagram of the UWB pulse generation scheme. EDFA: erbium-doped fiber amplifier; HNLF: highly nonlinear fiber; BPF: bandpass filter; VOA: variable optical attenuator; TDL: tunable delay line. ©2010 IEEE.

The electrical waveform at the balanced detector output can be expressed as:

$$V(t) \propto \left|E_{in}(t)\right|^2 - a_+ \left|E_+(t-t_+)\right|^2 - a_- \left|E_-(t-t_-)\right|^2 \tag{4}$$

where $a_\pm$ and $t_\pm$ are the relative power levels and delays of the leading and trailing edge waveforms, respectively. Unless corrected by the TDLs, the relative delays $t_\pm$ correspond to max (min) of the input intensity derivative. The complete waveform design requires a numeric calculation. Nonetheless, the following relations may serve as useful starting points: $t_+ = -t_- \approx \frac{1}{2}\tau_0$, $a_\pm \approx \frac{1}{2}\int\left|E_{in}(t)\right|^2 dt \Big/ \int\left|E_\pm(t)\right|^2 dt$. The central frequency f_C of $V(t)$ is on the order of $1/\left|t_2 - t_1\right|$, where $\left|t_2 - t_1\right|$ is the temporal width of the narrowed replica at the output of the edge detectors (see previous section).

Figure 4 shows a simulated example of the normalized shape of $V(t)$ (top panel) and its corresponding power spectral density $\left|\tilde{V}(\Omega)\right|^2$ (bottom), where Ω represents a radio frequency (RF) variable. The calculation parameters were the same as those of the previous section, with $a_\pm = 1.85$ and $t_\pm = \pm 10$ ps. The central frequency f_C of the high-order, UWB output waveform is 34 GHz. The high and low -10 dB cutoff frequencies $f_{H,L}$ are 47 GHz and 23 GHz, respectively, providing a fractional bandwidth $B_{fr} \equiv \left(f_H - f_L\right)/f_C$ of 70%. $V(t)$ can be simply modified through changing the peak power, width and shape of the incoming pulse train, the detuning of the BPFs, and the relative magnitude and delay of the replica trains of narrowed pulses. Experimental generation of UWB waveform is described next.

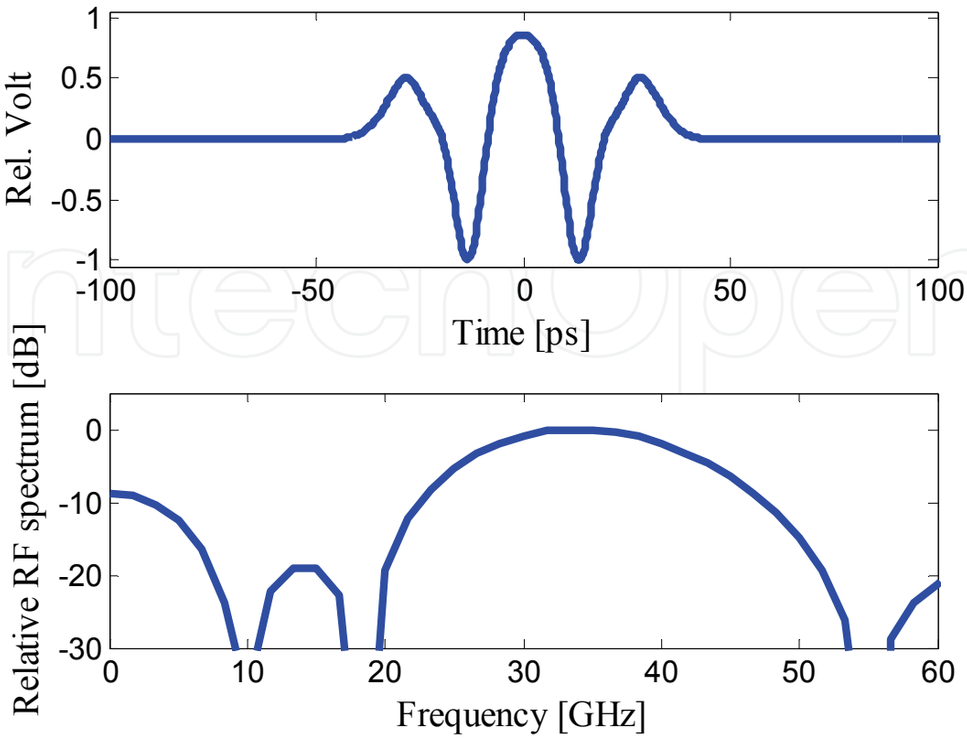

Fig. 4. Top – Simulated output waveform $V(t)$. The input pulse, HNLF and BPFs parameters are the same as those of Figs. 1 and 2, $a_{\pm} = 1.85$ and $t_{\pm} = \pm 10$ ps. Bottom – the corresponding RF spectrum $\left|\tilde{V}(\Omega)\right|^2$. ©2010 IEEE.

2.3 Experimental results

The generation of UWB pulses was demonstrated experimentally, using the setup of Fig. 3 (Zadok et al., 2010b, ©2010 IEEE). The parameters of the input pulse train and HNLF, and the settings of the BPFs, VOAs and TDLs were the same as those of the previous sections. The separation T_0 between neighboring pulses was 600 ps, corresponding to a data rate of 1.67 Gb/s. The average power of the amplified, input pulse train was 160 mW. Figure 5 shows the measured optical spectra $\left|\tilde{E}_{in}(\lambda)\right|^2$, $\left|\tilde{E}_{HNLF}(\lambda)\right|^2$ and $\left|\tilde{E}_{\pm}(\lambda)\right|^2$, corresponding to $E_{in}(t)$, $E_{HNLF}(t)$ and $E_{\pm}(t)$ respectively, as a function of wavelength λ.

Figure 6 (top) shows the measured $V(t)$ alongside the corresponding simulation. The experimental RF spectrum $\left|\tilde{V}(\Omega)\right|^2$, calculated by taking the Fourier transform of the measured $V(t)$, is shown at the bottom of Fig. 6 alongside the simulated results. The experimental waveform generally agrees with the simulation.

The flexibility of the waveform generation method is illustrated in Fig. 7 (Zadok et al., 2009; Zadok et al., 2010a), in which the setup parameters were adjusted to approximate the FCC mask for unlicensed indoor wireless UWB communication (FCC, 2002). In this experiment, Gaussian pulses (m = 2) of width τ_0 = 100 ps, peak power P_{in} = 1 W and spacing T_0 = 800 ps were used. Only a single edge detection BPF was used in the experiment, with a spectral width of 40 GHz and detuning $\Delta\omega/2\pi$ of 30 GHz. The normalized output waveform $V(t)$ approximates a Gaussian doublet pulse shape (top panel). The calculated $\left|\tilde{V}(\Omega)\right|^2$ is drawn

on the lower panel, alongside the FCC mask. The measurement generally complies with the mask requirements, although infringements can be seen at the lower frequency range.

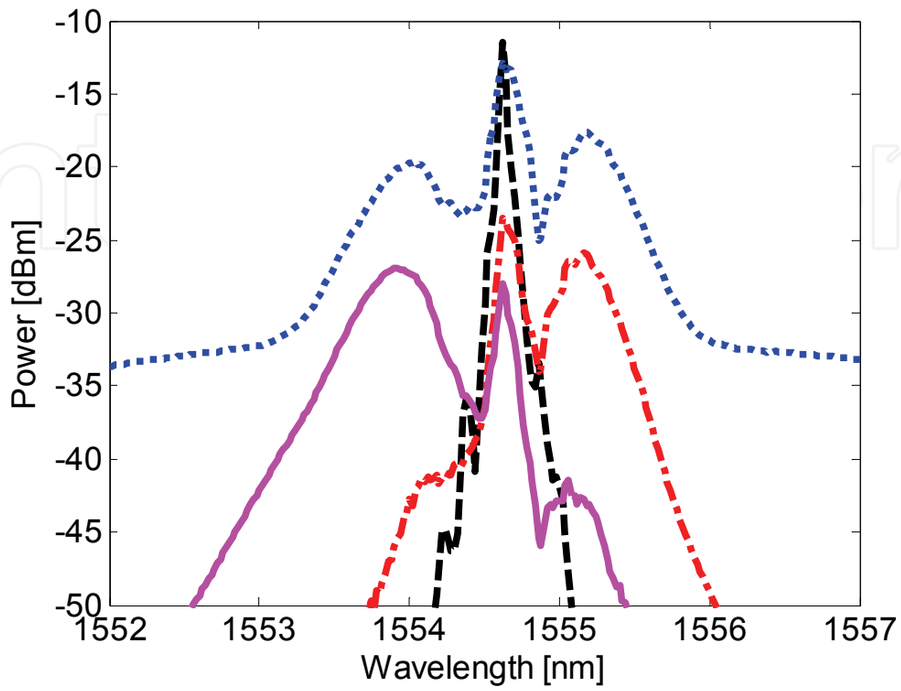

Fig. 5. Measured optical power spectra corresponding to $E_{in}(t)$ (dashed, black), $E_{HNLF}(t)$ (dotted, blue), $E_{+}(t)$ (solid, magenta) and $E_{-}(t)$ (dashed-dotted, red). The experimental parameters were the same as those of the simulations in Fig. 4. ©2010 IEEE.

The FCC mask infringements of the experimental Fig. 7 can be considerably reduced with the use of a narrower BPF: Figure 8 shows an example of simulated $V(t)$ and $\left|\tilde{V}(\Omega)\right|^2$ obtained with a single 10-GHz wide BPF. Results may be further improved by using two BPFs, as in Fig. 6.

2.4 Discussion and future work

The proposed technique for the photonic generation of UWB relies on all-optical detection of intensity edges of incoming super-Gaussian pulses. The technique could be particularly suitable for high-frequency waveforms, such as those intended for high-resolution vehicular radar systems. The edge detectors were implemented based on SPM in a section of HNLF, and using two BPFs in parallel. However, both edges might be detected simultaneously with the application of just one band-stop optical filter centered at ω_0, which would remove the center of the pulse (see Fig. 1). Data can be transmitted through simple on-off keying of the input pulses. On the other hand, pulse polarity modulation is not simply supported by the proposed approach.

The waveform generation setup includes multiple optical paths, the lengths of which were not matched in the experiment. The integrity of the UWB shape in a data-carrying, operational system could require path length equalization on mm scale. The problem might

be alleviated by using short fiber spans and high peak power levels, environmental isolation of fiber sections or active compensation. Alternatively, the relative delays $t_{\pm}$ could be controlled using dispersion rather than TDLs along different paths. The stability of the experimental setup was thus far validated over a couple of hours. Long term stability was not tested. The transmission of actual data using the proposed approach is the subject of further work.

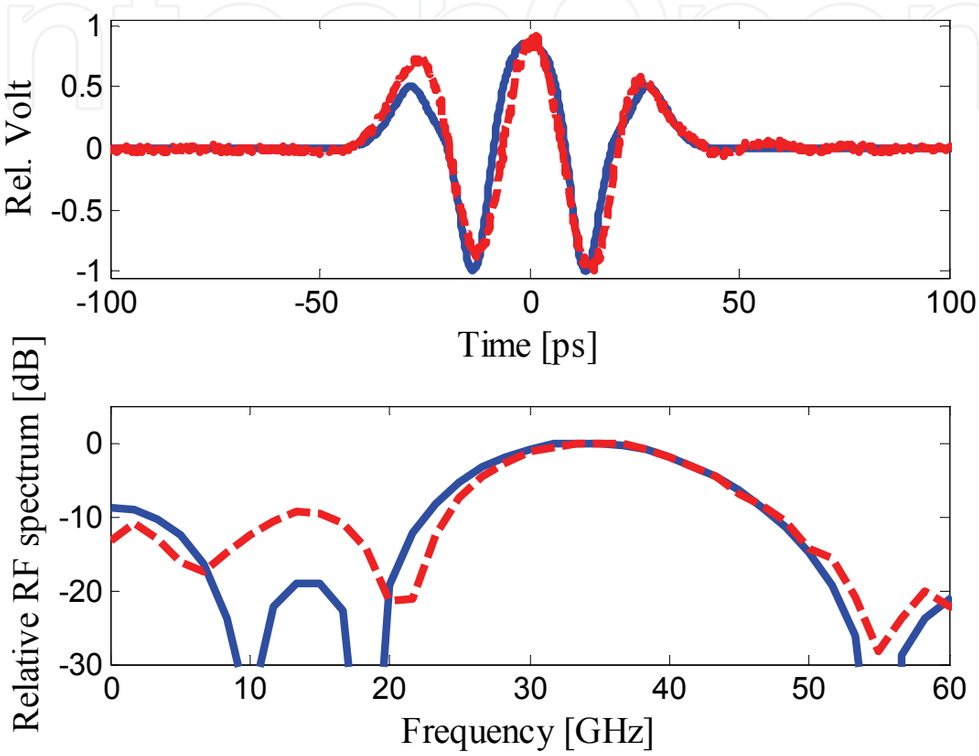

Fig. 6. Top – Simulated (solid, blue) and measured (dashed, red) output waveform $V(t)$. The experimental parameters were the same as those of the simulations in Fig. 4. Bottom – the corresponding simulated (solid, blue) and calculated experimental (dashed, red) RF spectra $|V(\Omega)|^2$. ©2010 IEEE.

The shaping and distribution scheme of the UWB pulses requires a two-fiber connection between a transmitter and a remote antenna element. Single-fiber transmission would be possible if a reference pulse shape $|E_{in}(t)|^2$ could be extracted from the SPM-broadened $E_{HNLF}(t)$ at the receiver. Ideally $|E_{HNLF}(t)|^2 = |E_{in}(t)|^2$, however residual dispersion and EDFA noise might distort the reference pulse shape. A potential solution might be narrow-band optical filtering centered at ω_0.

The comparison of the technique proposed in this work to previous approaches draws interesting analogies. Here, SPM introduces a time-to-frequency mapping, in which different temporal sections of the input pulses acquire different frequency shifts. This process is somewhat analogous to frequency-to-time mapping-based techniques (Abtahi et al., 2008a; McKinney et al., 2006; Wang et al., 2007), in which dispersion is used to assign a different delay to different spectral components of an input waveform. The subtraction of

the intensity profile of delayed replicas from the original pulse shape might be viewed as a tapped-delay line filtering method. It should be noted, though, that the subtracted waveforms are obtained through nonlinear processing and are not scaled copies of the input. The nonlinear propagation enables the generation of higher-order waveforms while using only two replicas, and also allows for simple reconfiguration through input power adjustments.

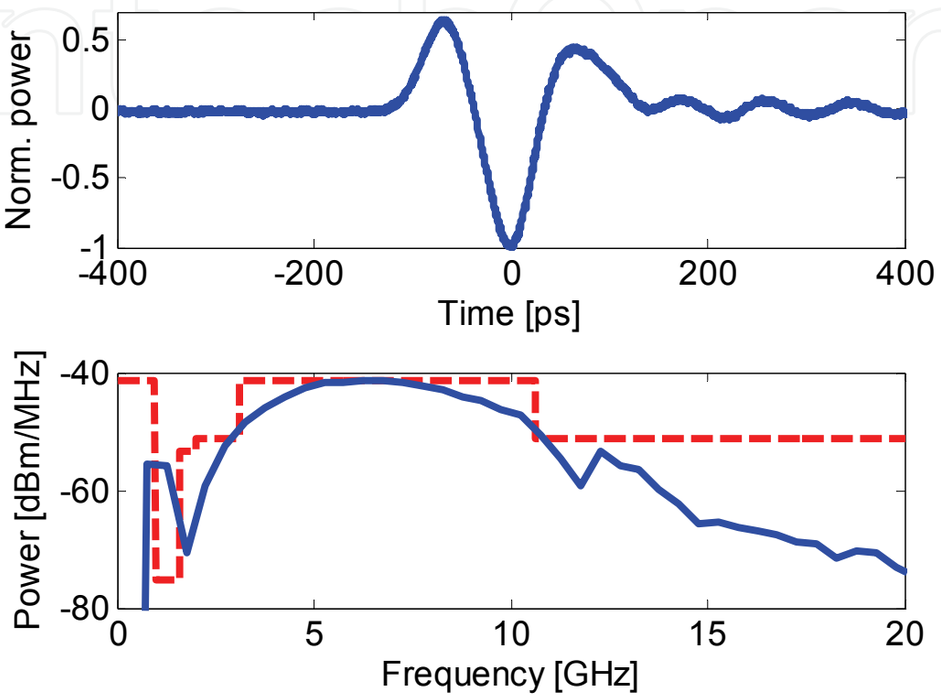

Fig. 7. Top– measured $V(t)$. Bottom– calculated experimental RF power spectrum $|V(\Omega)|^2$ (solid), alongside the FCC mask for indoor UWB communication (FCC, 2002) (dashed). Input parameters: P_{in} = 1 W, τ_0 = 100 ps , m = 2, T_0 = 800 ps. HNLF parameters: L = 1 km, γ = 11.3 [W·km]$^{-1}$. A single 40-GHz wide BPF was used, detuned by $\Delta\omega/2\pi$ = 30 GHz. ©2010 IEEE.

3. UWB noise waveforms generation using stimulated Brillouin scattering amplified spontaneous emission

As discussed above, impulse radio UWB communication requires elaborate pulse shaping, using either electrical or optical means. Alternatively, the criteria of UWB transmission may be met based on modulated noise waveforms, which could be simpler to generate. UWB noise communication had been previously proposed and demonstrated in several works (Haartsen et al., 2004; Haartsen et al., 2005; Narayanan & Chuang, 2007; Sahin et al., 2005). However, only few studies examined the use of optical techniques for noise generation. In one such recent example (Zheng et al., 2010), UWB noise was generated based on the chaotic dynamics of a laser diode within a fiber-optic feedback loop. UWB noise can be readily generated using electrical techniques (Upadhyaya, 1999), however optical methods are nonetheless appealing as part of a radio-over-fiber integrated system.

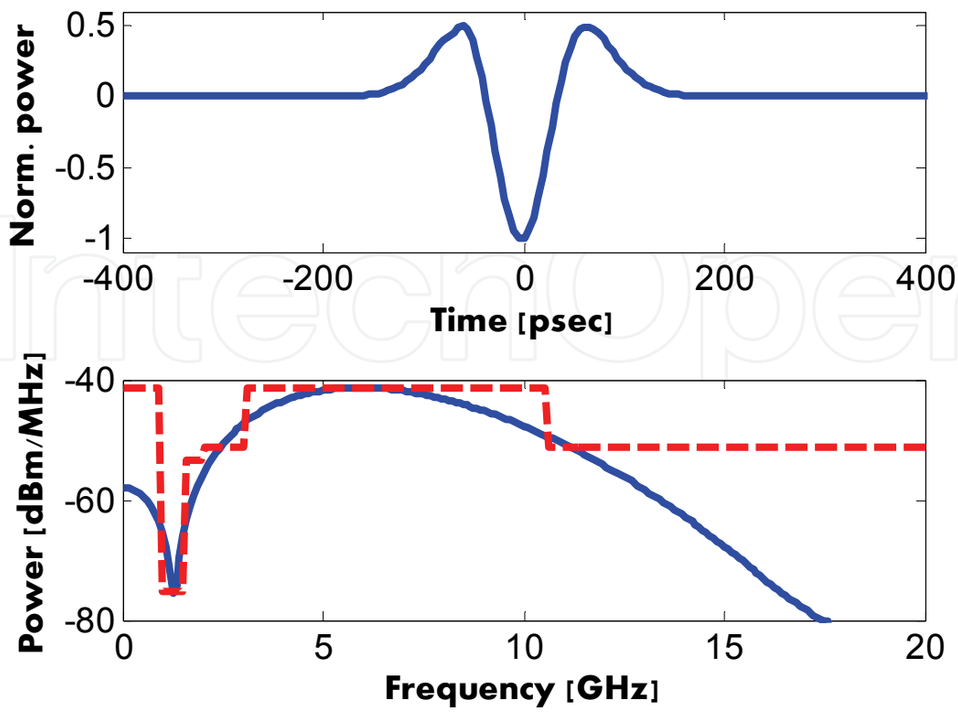

Fig. 8. Top– simulated $V(t)$. Bottom– corresponding simulated RF power spectrum $|V(\Omega)|^2$ (solid), alongside the FCC mask for indoor UWB communication (FCC, 2002) (dashed). Input pulses parameters: P_{in} = 1 W, τ_0 = 70 ps , m = 2. HNLF parameters: L = 1 km, γ = 11.3 [W·km]$^{-1}$. A single 10-GHz wide BPF was detuned from ω_0 by $\Delta\omega/2\pi$ = 20 GHz. ©2010 IEEE.

The rejection of interfering signals in UWB receivers relies on a proper matched filtering of incoming waveforms. The matched filter, in turn, requires precise knowledge of the transmitted pulse shapes and the transfer properties of the communication channel. In noise-based UWB schemes, a reference waveform must be provided to the receiver separately. In such transmit-reference (TR) techniques, an unmodulated replica of the data-carrying noise waveform is transmitted in parallel. Data and reference can by time-multiplexed, or launched at different intermediate frequencies or over two orthogonal polarizations (Narayanan and Chuang, 2007). TR UWB communication based on optically generated waveforms is demonstrated below.

3.1 Broadband noise generation

Stimulated Brillouin scattering (SBS) requires the lowest activation power of all non-linear effects in silica optical fibers. In SBS, a strong pump wave and a typically weak, counter-propagating signal wave optically interfere to generate, through electrostriction, a traveling longitudinal acoustic wave. The acoustic wave, in turn, couples these optical waves to each other (Boyd, 2008). The SBS interaction is efficient only when the difference between the optical frequencies of the pump and signal waves is very close (within a few tens of MHz) to a fiber-dependent parameter, the Brillouin shift Ω_B, which is of the order of 2π·11 GHz in silica fibers at room temperature and at 1550 nm wavelength (Boyd, 2008). An input signal

whose frequency is Ω_B lower than that of the pump, ('Stokes wave'), experiences SBS amplification. Among its numerous applications, SBS is used in optical processing of high frequency microwave signals (Loayssa et al., 2000; Loayssa & Lahoz, 2006; Loayssa et al., 2006; Shen et al., 2005; Zadok et al., 2007).

In the absence of a seed input signal wave, SBS could still be initiated by thermally-excited acoustic vibrations (Boyd, 2008). The naturally occurring vibrations scatter a fraction of the incident pump into a preliminary signal, which is then further amplified. In this scenario, SBS acts as a *generator* of amplified spontaneous emission (ASE) at the signal frequency. This SBS-ASE is the underlying mechanism of the UWB noise waveform generation described below. UWB generation requires a substantial spectral broadening of the inherently narrowband SBS process. Bandwidths of several GHz are routinely achieved through pump wave modulation (Zadok et al., 2007; Zhu et al., 2007).

A schematic drawing of a TR-assisted, SBS-ASE UWB noise transmitter is shown in Fig. 9 (Peled et al., 2010, ©2010 IEEE). Light from a distributed feedback (DFB) laser source is directly modulated and amplified. The spectrally broadened light is launched into a section of HNLF of length L and loss coefficient α as an SBS pump. Let us denote the generated, counter-propagating SBS-ASE noise field as $E_s(t)$. The power spectral density (PSD) of $E_s(t)$ is given by (Wang et al., 1996):

$$P(\omega_s) \propto \hbar\omega_s \left(\exp\left[g(\omega_s) L_{\text{eff}} - \alpha L \right] - 1 + \left[1 - \exp(-\alpha L) \right] \left\{ \exp\left[g(\omega_s) L_{\text{eff}} \right] - 1 \right\} \Big/ \left[g(\omega_s) L_{\text{eff}} \right] \right) \tag{5}$$

In (5) L_{eff} is the effective length of the fiber, and ω_s is the optical frequency of the generated Stokes wave. For a broadened pump, the SBS power gain coefficient $g(\omega_s)$, in units of m^{-1}, can be approximated as (Zadok et al., 2007; Zhu et al., 2007):

$$g(\omega_s) \propto P_p(\omega_s + \Omega_B) \tag{6}$$

where P_p denotes the pump PSD.

Careful synthesis of the pump laser direct modulation could provide a uniform P_p, and hence a uniform $P(\omega_s)$, within a range of several GHz (Zadok et al., 2007). The optical noise can be down-converted to the radio frequency (RF) domain through heterodyne beating with a local oscillator of frequency ω_{LO} on a broadband detector. The real-valued beating term $V(t)$ is proportional to a single ASE quadrature component, and is therefore of Gaussian statistics. Its PSD $\tilde{V}(\Omega)$ scales with $P(\omega_s = \Omega + \omega_{LO})$. The spectral width of $\tilde{V}(\Omega)$ is bounded by that of the pump.

3.2 Performance of transmit-reference UWB communication using SBS-ASE noise waveforms

In a TR-based implementation, the SBS-ASE noise field passes through an imbalanced Mach-Zehnder interferometer (MZI), with a differential delay of τ (see Fig. 9) (Peled et al., 2010, ©2010 IEEE). Light in the upper arm of the MZI is on/off modulated by information pulses of duration T_0. Following heterodyne down conversion, the electric signal to be transmitted can be expressed as:

$$V_{\mathrm{TR}}(t)=\sum_n a_n \mathrm{win}\left[\left(t-nT_0\right)/T_0\right]V(t)+V(t-\tau)\,, \tag{7}$$

where $\mathrm{win}(\xi)=1$ for $0<\xi\le 1$ and equals zero elsewhere, n is an integer and a_n is a binary data value. Data is recovered at the receiver by electrically mixing the incoming signal with a replica that is delayed by τ, and integrating over T_0:

$$Y[n]=\int_{nT0}^{(n+1)T0} V_{\mathrm{TR}}(t)V_{\mathrm{TR}}(t+\tau)\mathrm{d}t\,. \tag{8}$$

We require that $\tau << T_0$, in which case the decision variables for '1' and '0' are expressed as:

$$Y^{(1)}[n]=C_{V,T0,n}(0)+C_{V,T0,n}(\tau)+C_{V,T0,n}(-\tau)+C_{V,T0,n}(2\tau)\,. \tag{9}$$

$$Y^{(0)}[n]=C_{V,T0,n}(\tau) \tag{10}$$

where $C_{V,T0,n}(\xi)\equiv\int_{nT0}^{(n+1)T0} V(t)V(t+\xi)\mathrm{d}t$. Note that for $\tau << T_0$, $C_{V,T0,n}(\tau)\approx C_{V,T0,n}(-\tau)$. The ensemble averages of (9)-(10) are given by (Goodman, 2000):

$$I_1=\left\langle Y^{(1)}[n]\right\rangle_n=T_0\left[\Gamma_V(0)+2\Gamma_V(\tau)+\Gamma_V(2\tau)\right]\approx T_0\Gamma_V(0)\,. \tag{11}$$

$$I_0=\left\langle Y^{(0)}[n]\right\rangle_n=T_0\Gamma_V(\tau)<<I_1 \tag{12}$$

where $\Gamma_V(\xi)$ denotes the autocorrelation $\langle V(t)V(t+\xi)\rangle$. Equation (12) requires that τ is much longer than the coherence time τ_c of $V(t)$. Next the standard deviations $\sigma_{1,0}$ of equations (9)-(10) are estimated. Using the high-order moment theorem for real variables of Gaussian statistics (Goodman, 2000):

$$\begin{aligned}\sigma^2_{V,T0}(\xi)&\equiv\left\langle C^2_{V,T0,n}(\xi)\right\rangle_n-\left\langle C_{V,T0,n}(\xi)\right\rangle_n^2\\&=\iint_{T0}\left[\Gamma_V(t-t')\right]^2\mathrm{d}t\mathrm{d}t'+\iint_{T0}\Gamma_V(t-t'-\xi)\Gamma_V(t-t'+\xi)\mathrm{d}t\mathrm{d}t'\end{aligned}\,. \tag{13}$$

For $T_0>>\tau_c$, the first term of (13) equals $T_0\tau_c\left[\Gamma_V(0)\right]^2$ (Goodman, 2000). The second term reduces to the first for $\xi\approx 0$, and vanishes for $\xi>>\tau_c$. Using equations (9), (10) and (13):

$$\sigma_1^2=\sigma^2_{V,T0}(0)+4\sigma^2_{V,T0}(\tau)+\sigma^2_{V,T0}(2\tau)=7\tau_c T_0\left[\Gamma_V(0)\right]^2\,, \tag{14}$$

$$\sigma_0^2=\tau_c T_0\left[\Gamma_V(0)\right]^2\,. \tag{15}$$

The Q parameter for UWB communication based on Gaussian noise with TR is given by:

$$Q_{\mathrm{TR}}=\left(I_1-I_0\right)/\left(\sigma_1+\sigma_0\right)=\sqrt{T_0/\tau_c}\Big/\left(\sqrt{7}+1\right)=0.27\sqrt{T_0/\tau_c}\,. \tag{16}$$

The corresponding value for direct detection equals:

$$Q_{\mathrm{dir}}=\tfrac{1}{\sqrt{2}}\sqrt{T_0/\tau_c}=2.58Q_{\mathrm{TR}}\,. \tag{17}$$

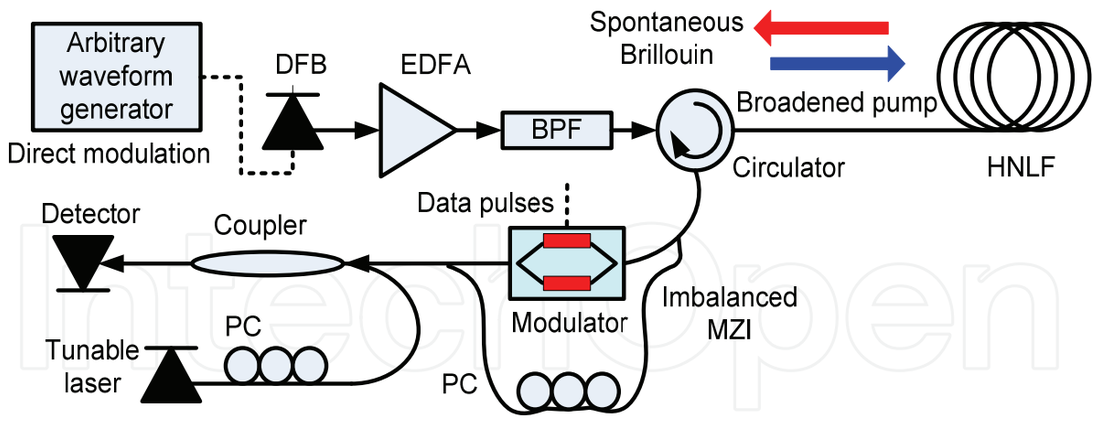

Fig. 9. Setup for a transmit-reference, ultra-wideband noise transmitter based on the amplified spontaneous emission of Brillouin scattering. DFB: distributed feedback laser; EDFA: erbium-doped fiber amplifier; BPF: band-pass filter; HNLF: highly nonlinear fiber; PC: polarization controller; MZI: Mach-Zehnder Interferometer. ©2010 IEEE.

3.3 Experimental demonstration of UWB communication

UWB noise generation based on SBS-ASE and its coherent detection were demonstrated experimentally. Light from a DFB laser was directly modulated by an arbitrary waveform generator (see Fig. 9) (Peled et al., 2010, ©2010 IEEE). The modulating waveform was (Zadok et al., 2007):

$$i(t) = i_0 - \Delta i\left(t \bmod T_p / T_p\right)^{2.1}, \tag{18}$$

where T_p = 500 ns is the modulation period, i_0 = 80 mA is the DFB bias current and Δi ~ 7.5 mA is the modulation magnitude. A heterodyne measurement of the modulated DFB PSD is shown in Fig. 10 (top). The DFB output was amplified to 250 mW by an EDFA, and launched into 3.5 km of HNLF (α = 1 dB/km) as an SBS pump wave. Fig. 10 (center) shows the PSD $\tilde{V}(\Omega)$ of the down-converted SBS-ASE noise. $\tilde{V}(\Omega)$ is uniform within a range of 1.1 GHz. The arbitrary central frequency of 2.4 GHz was chosen due to equipment limitations. $\tilde{V}(\Omega)$ can be broadened beyond 10 GHz with stronger pump amplification (Zhu et al., 2007), hence no fundamental limitations prevent the compliance of the noise waveform with the FCC standard. Fig. 10 (bottom) shows a histogram of $V(t)$, alongside a Gaussian distribution of equal variance. The SBS-ASE noise is well described by Gaussian statistics. $\tau_c \equiv \int_{-\infty}^{\infty}\left[\Gamma_V(\xi)\right]^2 d\xi \Big/ \left[\Gamma_V(0)\right]^2$ of 0.45 ns was directly calculated from samples of $V(t)$ (Goodman, 2000).

The SBS-ASE optical field was modulated by square waves using an electro-optic modulator. First, the lower arm of the MZI was disconnected, and the modulated noise was directly detected. Fig. 11 (top) shows an example of the detected waveform with T_0 = 112 ns. Q_{dir} was estimated by sampling $V(t)$ over several hundred periods, and calculating equation (8) with τ = 0. The results for T_0 = 112 and 225 ns were Q_{dir} = 10 and 14.7, respectively. The results agree with the predicted values of 11.1 and 15.8. The differences could be due to the finite extinction ratio of the modulator and additive detector noise.

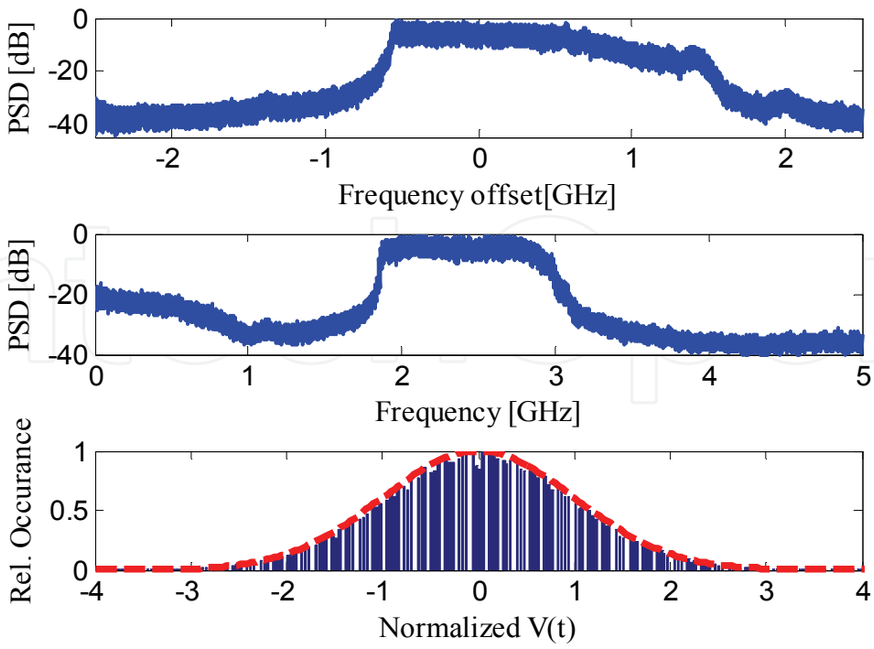

Fig. 10. Top – Power spectral density (PSD) of the directly modulated stimulated Brillouin scattering (SBS) pump wave. Center – PSD of the down-converted SBS amplified spontaneous emission (SBS-ASE) $\tilde{V}(\Omega)$. Bottom - Histogram of the down-converted SBS-ASE noise $V(t)$ (bar), alongside a zero-mean Gaussian distribution of equal variance (line). ©2010 IEEE.

TR-assisted coherent detection of UWB noise communication was demonstrated by reconnecting the lower arm of the MZI with τ of 12.2 ns. Fig. 11 (center) shows an example of $V_{TR}(t)$ and the bottom panel shows its autocorrelation. A secondary peak corresponding to τ is evident. Fig. 12 shows an example of the calculated experimental histogramsof $Y^{(1)}[n]$ and $Y^{(0)}[n]$. The estimated Q_{TR} values for T_0 = 112 and 225 ns were 3.25 and 4.6, respectively. Based on the experimental values of Q_{dir}, equation (17) suggests a Q_{TR} of 3.9 and 5.7 for the two symbol durations. The difference may stem from unequal power splitting in the MZI or residual statistical correlation among the terms of $Y^{(1)}[n]$ (see equation (9)).

3.4 UWB noise radar based on SBS-ASE

The SBS-ASE UWB noise waveforms discussed above were also used in a proof-of-concept radar measurement. To that end, the generated waveform $V(t)$ was split in two branches. The waveform in one branch was amplified to -5 dBm and transmitted by a horn antenna with a gain of 20 dBi. The waveform was reflected from a 40X40 cm² metallic object at different distances. The reflections were collected by a second, identical antenna, amplified and sampled by a real-time digitizing oscilloscope with a bandwidth of 6 GHz. A replica of $V(t)$ in the other arm was sampled by a second oscilloscope channel as a reference. The correlation function between the two sampled waveforms was calculated, and the distance to the target was estimated based on the timing of the observed correlation peak. Figure 13

shows the measured correlation for several target distances. The full width at half-maximum of the correlation peaks suggests an estimated resolution of 20 cm, in good agreement with the expected value of 15 cm for a 1 GHz-wide noise waveform.

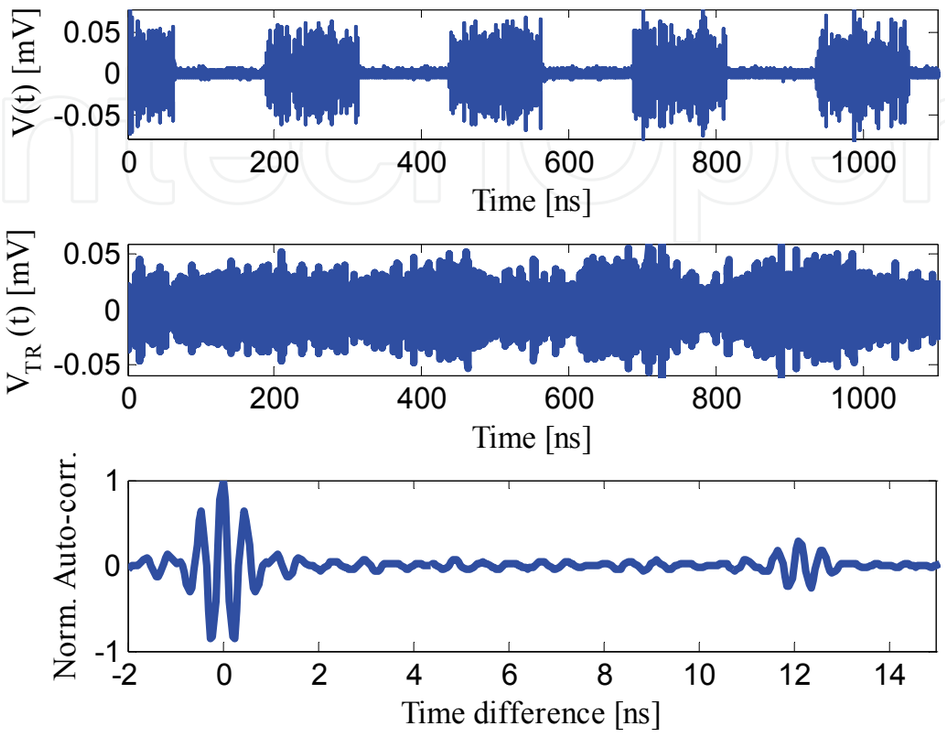

Fig. 11. Top – Measured modulated noise $V(t)$ with no transmitted reference, symbol duration T_0 = 112 ns. Center – Measured $V_{TR}(t)$ with a transmitted reference, T_0 = 112 ns, relative delay τ = 12.2 ns. Bottom- Normalized autocorrelation of $V_{TR}(t)$ (T_0 ,τ as above). ©2010 IEEE.

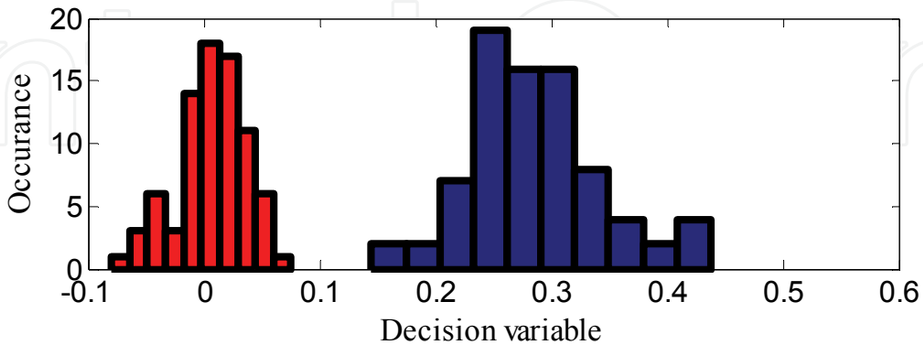

Fig. 12. Experimental histograms of the decision variable $Y[n]$ for ultra-wideband noise communication with a transmitted reference, based on amplified spontaneous emission from Brillouin scattering. T_0 = 112 ns, τ = 12.2 ns Left: logical '0'. Right: logical '1'. Histograms consist of 160 symbols. ©2010 IEEE.

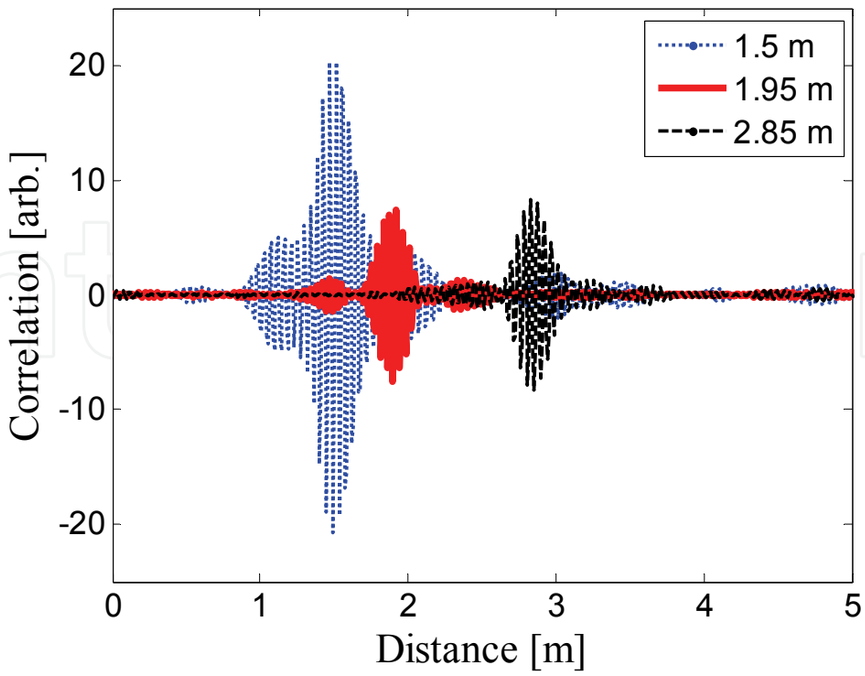

Fig. 13. Measured correlation between a UWB noise waveform reflected from a metal target and a reference replica. The transmitted 1 GHz-wide noise waveforms were optically generated using SBS-ASE. The distances to the target were 1.5 m (blue, dotted); 1.95 m (red, solid) and 2.85 m (black, dahsed).

4. Concluding remarks

In this chapter, nonlinear propagation over optical fibers was used for the generation of UWB waveforms. Two different nonlinear mechanisms had been employed: SPM and SBS. The generation of both UWB impulse radio shapes and UWB noise had been demonstrated. Impulse radio pulse shapes were generated based on SPM. The technique relied on the time-to-frequency mapping that accompanies SPM spectral broadening of pulses, in implementing all-optical edge detectors. The edge detectors provided temporally-narrowed replicas of an input train of standard pulses. The shapes of the narrow replicas were later electrically subtracted from that of the original pulses by a differential detector. The method provides multiple degrees of freedom for shaping high-order UWB waveforms of high central radio frequencies, up to 34 GHz. Noise waveforms were generated based on the ASE that accompanies SBS in fiber. The ASE noise bandwidth was broadened to 1.1 GHz via pump modulation. The method is readily extendable to the generation of waveforms having arbitrary central radio frequencies, and widths approaching 10 GHz. The noise waveforms were used in proof-of-concept demonstrations of transmit-reference UWB communication and UWB noise radar.

The techniques reported rely on off-the-shelf components only. Few of the components included in the experimental setups, such as EDFA, HNLF or differential detector, are currently too expensive for certain applications. Higher cost may be more tolerable in applications in which a single transmitter is broadcasting to a large number of simple receivers, or where waveforms of high-order and high-frequency are required.

A primary motivation which is driving microwave photonics research in general, and UWB-related photonic techniques in particular, is the potential for a radio-over-fiber integrated system which brings together fiber-optic distribution and broadband all-optical processing. In this respect, techniques which employ the fiber itself as the waveform-generating medium stand out. Future work will be dedicated to advance the proposed methods towards applications.

5. References

Abtahi, M.; Mirshafiei, M.; Magne, J.; Rusch, L. A. & LaRochelle, S. (2008a). Ultra-wideband waveform generator based on optical pulse-shaping and FBG tuning. *IEEE Photonics Technology Letters*, Vol. 20, No. 2, (January 2008), pp. 135-137, ISSN 1041-1135.

Abtahi, M.; Magne, J.; Mirshafiei, M.; Rusch, L.A. & LaRochelle, S. (2008b). Generation of Power-Efficient FCC-Compliant UWB Waveforms Using FBGs: Analysis and Experiment. *Journal of Lightwave Technology,* Vol. 26, No. 5, (March 2008), pp. 628-635, ISSN 0733-8724.

Abtahi, M.; Mirshafiei, M.; LaRochelle, S. & Rusch, L.A. All-Optical 500-Mb/s UWB Transceiver:An Experimental Demonstration (2008c). *Journal of Lightwave Technology*, Vol. 26, No. 15, (August 2008), pp. 2795-2802, ISSN 0733-8724.

Ben-Ezra, Y. ; Lembrikov, B. I. & Haridim, M. (2009). Ultrafast All-Optical Processor Based on Quantum-Dot Semiconductor Optical Amplifiers. *IEEE Journal of Quantum Electronics*, Vol. 45, No. 1-2, (January 2009), pp. 34-41, ISSN 0018-9197.

Bolea, M.; Mora, J.; Ortega, B. & Capmany, J. (2009). Optical UWB pulse generator using an N tap microwave photonic filter and phase inversion adaptable to different pulse modulation formats. *Optics Express*, Vol. 17, No. 7, (March 2009), pp. 5021-5032, eISSN 1094-4087.

Bolea, M.; Mora, J.; Ortega, B.; & Capmany, J. (2010). Flexible Monocycle UWB Generation for Reconfigurable Access Networks (2010). *IEEE Photonics Technology Letters*, Vol. 22, No. 12, (May 2010), pp. 878-880, ISSN 1041-1135.

Boyd, R. W. (2008). *Nonlinear optics*, third edition, Academic Press, ISBN 978-0-12-369470-6, San Diego, CA.

Capmany, J.; Ortega, B.; Pastor, D. & Sales, S. (2005). Discrete-time optical processing of microwave signals. *Journal of Lightwave Technology*, Vol. 23, No. 2, (February 2005), pp. 702-723, ISSN 0733-8724.

Chow, C. W.; Kuo, F. M.; Shi, J. W.; Yeh, C. H.; Wu, Y. F.; Wang, C. H.; Li, Y. T. & Pan, C. L. (2010). 100 GHz ultra-wideband (UWB) fiber-to-the antenna (FTTA) system for in-building and inhome networks. *Optics Express*, Vol. 18, No. 2, (January 2010), pp. 473-478, eISSN 1094-4087.

Chuang, J.; DeMay, M. W. & Narayanan, R. M. (2008). Design, Analysis, and Performance of a Noise Modulated Covert Communications System. *EURASIP Journal on Wireless Communications and Networking*, Vol. 2008, (July 2008), Article ID 979813, eISSN 1687-1499.

Gibbon, T.B.; Yu, X; Gamatham, R; Guerrero Gonzalez, N; Rodes, R; Bevensee Jensen, J; Caballero, A & Monroy I. T. (2010). 3.125 Gb/s Impulse Radio Ultra-Wideband

Photonic Generation and Distribution Over a 50 km Fiber With Wireless Transmission. *IEEE Microwave and Wireless Components Letters,* Vol. 20, No. 2, (February 2010), pp. 127-129, ISSN 1531-1309.

Goodman, J. W. (2000). *Statistical Optics*, Wiley Classics Library Edition, ISBN 0-471-39916-7, New York, NY.

Haartsen, J. C.; Meijerink, A.; Bekkaoui, A.; Taban, A. & Tauritz, J. L. (2004). Novel wireless modulation technique based on noise. *Proceedings of IEEE 11th Symposium on Communications and Vehicular Technology in the Benelux (SCVT 2004),* Ghent, Belgium.

Haartsen, J. C.; Shang, X.; Balkema, J. W.; Meijerink, A. & Tauritz, J. L. (2005). A new wireless modulation scheme based on frequency-offset. *Proceedings of IEEE 12th Symposium on Communications and Vehicular Technology in the Benelux (SCVT 2005),* Enschede, the Netherlands.

Hanawa, M.; Mori, K.; Nakamura, K.; Matsui, A. & Nonaka, K. (2010). Experimental demonstration of high-resolution ultra-wideband impulse radar based on electrical-optical hybrid pulse generation. *IET Microwaves, Antennas and Propagation,* Vol. 4, No. 10 (October 2010), pp. 1462-1468, ISSN 1751-8725.

Khan, M.; Shen, H.; Xuan, Y.; Zhao, L.; Xiao, S.-J.; Leaird, D. E.; Weiner, A. M. & Qi, M. H. (2010). Ultrabroad-bandwidth arbitrary radiofrequency waveform generation with silicon photonic chip-based spectral shaper. *Nature Photonics,* Vol. 4, No. 2, (February 2010), pp. 117-U30, ISSN 1749-4885.

Li, J.; Kuo, B. P.-P. & Wong, K. K.-Y. (2009). Ultra-wideband pulse generation based on cross-gain modulation in fiber optical parametric amplifier. *IEEE Photonics Technology Letters,* Vol. 21, No. 4, (February 2009), pp. 212-214, ISSN 1041-1135.

Loayssa, A.; Benito, B. & Grade, M. J. (2000). Optical carrier-suppression technique with a Brillouin-erbium fiber laser. *Optics Letters*, Vol. 25, No. 4, (February 200), pp. 197-199, ISSN 0146-9592.

Loayssa, A. & Lahoz, F. J. (2006). Broadband RF photonic phase shifter based on stimulated Brillouin scattering and single side-band modulation. *IEEE Photonics Technology Letters,* Vol. 18, No. 1, (January 2006), pp. 208-210, ISSN 1041-1135.

Loayssa, A.; Capmany, J.; Sagues, M. & Mora, J. (2006). Demonstration of incoherent microwave photonic filters with all-optical complex coefficients. *IEEE Photonics Technology Letters,* Vol. 18, No. 16, (August 2006), pp. 1744-1746, ISSN 1041-1135.

McKinney, J. D.; Lin, I. S. & Weiner, A. M. (2006). Shaping the power spectrum of ultra-wideband radio-frequency signals. *IEEE Transactions on Microwave Theory and Techniques*, Vol. 54, No. 12 part 1, (December 2006), pp. 4247-4255, ISSN 0018-9480.

McKinney, J. D. (2010). Background-Free Arbitrary Waveform Generation via Polarization Pulse Shaping. *IEEE Photonics Technology Letters,* Vol. 22, No. 16, (August 2010), pp. 1193-1195, ISSN 1041-1135.

Narayanan, R. M. & Chuang, J. (2007). Covert communication using heterodyne correlation random noise signals. *Electronics Letters,* Vol. 43, No. 22, (October 2007), pp. 1211-1212, ISSN 0013-5194.

Narayanan, R. M. (2008). Through-wall radar imaging using UWB noise waveforms. *Journal of the Franklin Institute,* Vol. 345, No. 6, (September 2008), pp. 659-678, ISSN 0016-0032.

Peled, Y.; Tur, M. & Zadok, A. (2010). Generation and Detection of Ultra-Wideband Waveforms Using Stimulated Brillouin Scattering Amplified Spontaneous Emission. *IEEE Photonics Technology Letters,* Vol. 22, No. 22, (November 2010), pp. 1692-1694, ISSN 1041-1135.

Pham, T.-T.; Yu, X.; Dittmann, L. & Monroy, I. T. (2011). Integration of Optically Generated Impulse Radio UWB Signals into Baseband WDM-PON. Accepted for publication in *IEEE Photonics Technology Letters,* Vol. 23, (2011), ISSN 1041-1135.

Qiu. R. C.; Liu, H. & Shen, X. (2005). Ultra-wideband for multiple access communication. *IEEE Communications Magazine*, Vol. 43, No. 2, (February 2005), pp. 80-87, ISSN 0163-6804.

Sahin, M. E.; Guvenc, I. & Arslan, H. (2005). Optimization of energy detector receivers for UWB systems. *Proceedings of the IEEE 61st Vehicular Technology Conference*, Stockholm, Sweden, Vol. 2, (May-June 2005), pp. 1386-1390 ISSN 1550-2252.

Shen, Y.; Zhang, X. & Chen, K. (2005). Optical single side-band modulation of 11 GHz RoF system using stimulated Brillouin scattering. *IEEE Photonics Technology Letters* Vol. 17, No. 6, (June 2005), pp. 1277-1279, ISSN 1041-1135.

United States Federal Communication Commission (FCC). (2002). Technical report ET-Docket 98-153, FCC02-48, (April 2002).

Upadhyaya, S. J. (1999). Noise Generators. *Wiley Encyclopedia Electrical and Electronics Engineering*. Online ISBN: 9780471346081, New York, NY.

Velanas, P.; Bogris, A.; Argyris, A. & Syvridis, D. (2008). High-speed all-optical first- and second-order differentiators based on cross-phase modulation in fibers. *Journal of Lightwave Technology*, Vol. 26, No. 18, (September 2008), pp. 3269-3276, ISSN 0733-8724.

Wang, C.; Zeng, F. & Yao, J. P. (2007). All-fiber ultrawideband pulse generation based on spectral shaping and dispersion-induced frequency-to-time conversion. *IEEE Photonics Technology Letters,* Vol. 22, No. 3, (February 2007), pp. 137-139, ISSN 1041-1135.

Wang, J.; Tang, W. and Zhu, W. (1996). Stimulated Brillouin scattering initiated by thermally excited acoustic waves in absorption media. *Optics Communications*, Vol. 123, No. 4-6, (February 1996), pp. 574-576, ISSN 0030-4018.

Wu, T.-H.; Wu, J.-P. & Chiu, Y.-J. (2010). Novel Ultra-wideband (UWB) photonic generation through photodetection and crossabsorption modulation in a single electroabsorption modulator. *Optics Express*, Vol. 18, No. 4, (February 2010), pp. 3379-3384, eISSN 1094-4087.

Xu, J.; Zhang, X.; Dong, J.; Liu, D. & Huang, D. (2007a). High-speed all-optical differentiator based on a semiconductor optical amplifier and an optical filter. *Optics Letters,* Vol. 32, No. 13, (July 2007), pp. 1872-1874, ISSN 0146-9592.

Xu, J.; Zhang, X.; Dong, J.; Liu, D. & Huang, D. (2007b). All-optical differentiator based on cross-gain modulation in semiconductor optical amplifier. *Optics Letters,* Vol. 32, No. 20, (October 2007), pp. 3029-3031, ISSN 0146-9592.

Yang, L. & Giannakis, G. B. (2004). Ultra-wideband communications: an idea whose time has come. *IEEE Signal Processing Magazine*, Vol. 21, No. 6, (November 2004), pp. 26-54, ISSN 1053-5888.

Yao, J.; Zeng, F. & Wang, Q. (2007). Photonic generation of ultrawideband signals. *Journal of Lightwave Technology*, Vol. 25, No. 11, (November 2007), pp. 3219-3235, ISSN 0733-8724.

Yu, X.; Gibbon, T. B.; Pawlik, M.; Blaaberg, S. & Monroy, I. T. (2009). A photonic ultra-wideband pulse generator based on relaxation oscillations of a semiconductor laser. *Optics Express,* Vol. 17, No. 12, (June 2009), pp. 9680-9687 eISSN 1094-4087.

Zadok, A.; Eyal, A. & Tur, M. (2007). GHz-wide optically reconfigurable filters using stimulated Brillouin scattering. *Journal of Lightwave Technology,* Vol. 25, No. 8, (August 2007), pp. 2168-2174, ISSN 0733-8724.

Zadok, A.; Wu, X.; Sendowski, J.; Yariv, A. & Willner, A. E. (2009). Flexible All-Fiber Generation of Ultra-Wideband Signals via Pulse Compression and Differential Detection. Paper FWK3 in *Proceedings of Frontiers in Optics* San-Jose, CA October 2009.

Zadok, A.; Wu, X.; Sendowski, J.; Yariv, A. & Willner, A. E. (2010a). Photonic generation of ultra-wideband signals via pulse compression in a highly nonlinear fiber. *IEEE Photonics Technology Letters,* Vol. 22, No. 4, (February 2010), pp. 239-241, ISSN 1041-1135.

Zadok, A.; Wu, X.; Sendowski, J.; Yariv, A. & Willner, A. E. (2010b). Reconfigurable generation of high-order ultra-wideband waveforms using edge detection," *Journal of Lightwave Technology*, Vol. 28, No. 16, (August 2010), pp. 2207-2012, ISSN 0733-8724.

Zeng, F. & Yao, J. P. (2006). Ultrawideband signal generation using a high-speed electrooptic phase modulator and an FBG-based frequency discriminator. *IEEE Photonics Technology Letters* Vol. 18, No. 19, (October 2006), pp. 2062–2064, ISSN 1041-1135.

Zeng, F.; Wang, Q. & Yao, J. P. (2007). All-optical UWB impulse generation based on cross phase modulation and frequency discrimination. *Electronics Letters*, Vol. 43, No. 2, (January 2007), pp. 119–121, ISSN 0013-5194.

Zheng, J.-Y.; Zhang, M.-J.; Wang, A.-B. & Wang, Y.-C. (2010). Photonic generation of ultrawideband pulse using semiconductor laser with optical feedback. *Optics Letters,* Vol. 35, No. 11 (June 2010), pp. 1734-1736, ISSN 0146-9592.

Zhu, Z.; Daws, A. M. C.; Gauthier, D. J.; Zhang, L. & Willner, A. E. (2007). Broadband SBS slow light in an optical fiber. *Journal of Lightwave Technology*, Vol. 25, No. 1, (January 2007), pp. 201-206, ISSN 0733-8724.

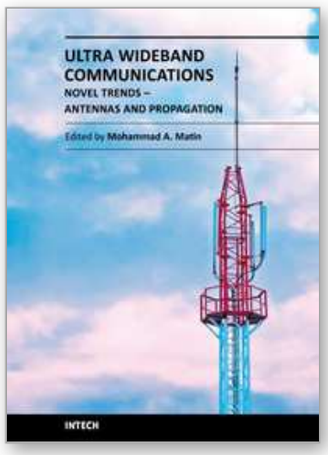

Ultra Wideband Communications: Novel Trends - Antennas and Propagation

Edited by Dr. Mohammad Matin

ISBN 978-953-307-452-8
Hard cover, 384 pages
Publisher InTech
Published online 09, August, 2011
Published in print edition August, 2011

This book explores both the state-of-the-art and the latest achievements in UWB antennas and propagation. It has taken a theoretical and experimental approach to some extent, which is more useful to the reader. The book highlights the unique design issues which put the reader in good pace to be able to understand more advanced research.

How to reference

In order to correctly reference this scholarly work, feel free to copy and paste the following:

Avi Zadok, Daniel Grodensky, Daniel Kravitz, Yair Peled, Moshe Tur, Xiaoxia Wu and Alan E. Willner (2011). Ultra-Wideband Waveform Generation Using Nonlinear Propagation in Optical Fibers, Ultra Wideband Communications: Novel Trends - Antennas and Propagation, Dr. Mohammad Matin (Ed.), ISBN: 978-953-307-452-8, InTech, Available from: http://www.intechopen.com/books/ultra-wideband-communications-novel-trends-antennas-and-propagation/ultra-wideband-waveform-generation-using-nonlinear-propagation-in-optical-fibers

INTECH
open science | open minds

InTech Europe
University Campus STeP Ri
Slavka Krautzeka 83/A
51000 Rijeka, Croatia
Phone: +385 (51) 770 447
Fax: +385 (51) 686 166
www.intechopen.com

InTech China
Unit 405, Office Block, Hotel Equatorial Shanghai
No.65, Yan An Road (West), Shanghai, 200040, China
中国上海市延安西路65号上海国际贵都大饭店办公楼405单元
Phone: +86-21-62489820
Fax: +86-21-62489821

IntechOpen